

Evidence of octupole correlation in ^{79}Se

S. Rajbanshi^{1,*}, R. Palit,² R. Raut,³ Y. Y. Wang,⁴ Z. X. Ren⁴, J. Meng,⁴ Q. B. Chen,⁵ Sajad Ali,⁶ H. Pai^{7,†}, F. S. Babra,² R. Banik,^{8,9} S. Bhattacharya,¹⁰ S. Bhattacharyya^{9,11}, P. Dey,² S. Malik,¹ G. Mukherjee,^{9,11} Md. S. R. Laskar², S. Nandi^{9,11}, Rajkumar Santra,^{7,9} T. Trivedi,¹⁰ S. S. Ghugre,³ and A. Goswami⁷

¹Presidency University, Kolkata 700073, India

²Tata Institute of Fundamental Research, Mumbai 400005, India

³UGC-DAE-Consortium for Scientific Research, Kolkata 700098, India

⁴State Key Laboratory of Nuclear Physics and Technology, School of Physics, Peking University, Beijing, 100871, China

⁵Department of Physics, East China Normal University, Shanghai 200241, China

⁶Government General Degree College at Pedong, Kalimpong 734311, India

⁷Saha Institute of Nuclear Physics, 1/AF, Bidhannagar, Kolkata 700064, India

⁸Institute of Engineering and Management, Saltlake Sector V, Kolkata 700091, India

⁹Homi Bhabha National Institute, Training School Complex, Anushakti Nagar, Mumbai 400094, India

¹⁰Department of Pure & Applied Physics, Guru Ghasidas Vishwavidyalaya, Bilaspur 495009, India

¹¹Variable Energy Cyclotron Center, Kolkata 700064, India



(Received 25 January 2021; revised 5 November 2021; accepted 1 December 2021; published 17 December 2021)

Two opposite parity bands I and II with eight new parity changing transitions have been identified in ^{79}Se using the fusion-evaporation reaction $^{76}\text{Ge}(^9\text{Be}, \alpha 2n)$ at $E_{\text{Lab}} \approx 31$ MeV. The $B(M1)$ and $B(E2)$ rates of bands I and II as well as $B(E1)$ values of the linking transitions between the two bands have been determined from lifetime measurements and are compared with reflection asymmetric triaxial particle rotor model calculations. The large $B(E1)/B(E2)$ ratios and $B(E1)$ transition rates indicate the existence of a strong octupole correlation in the ^{79}Se nucleus. This is also supported by the calculated potential energy surface, based on the covariant density functional theory within the three-dimensional lattice approach, which is very soft for the octupole shape degree of freedom β_{30} . Extracted values of the intrinsic dipole moments $|D_0|$ from the $B(E1)$ rates for the lower spin states also indicate the octupole correlation in ^{79}Se .

DOI: [10.1103/PhysRevC.104.064316](https://doi.org/10.1103/PhysRevC.104.064316)

I. INTRODUCTION

The concept of spontaneous symmetry breaking plays a crucial role in understanding the underlying modes of excitation associated with the many-body quantum (fermions) system [1,2]. Such multipole modes of excitation depend on the occupancy of the valence particles in the particular orbitals, which leads to various nuclear shapes. Observation of large quadrupole moments of rotational band structures leads to the deformed shape of the nucleus. For most deformed nuclei, a description as an axial- and reflection-symmetric spheroid is adequate to reproduce the band's spectroscopy. However, reflection-asymmetric shapes can also play a role in the excitation mechanism, though they are not as stable as the familiar quadrupole deformations [3]. Such a reflection-asymmetric shape of a nucleus is the consequence of the octupole-octupole interactions.

The pairs of the opposite-parity orbitals near the Fermi surface with $\Delta l = \Delta j = 3\hbar$ form the necessary condition for exhibiting the nuclear octupole collectivity. Intrinsic reflection symmetry breaking in a nucleus occurs due to either the static octupole deformation or the dynamic octupole correlation. The octupole-deformed shapes of the nuclei produce permanent electric-dipole moments of the atoms that provide significant constraints on many proposed extensions to the standard model [4]. The odd-A octupole-deformed nuclei show a higher Schiff moment that is a measure of nuclear time-reversal violation that is particularly enhanced [5].

For the even-even nuclei, the low-lying 3^- state is observed in their excitation spectrum. The odd-nuclei exhibit a pair of almost degenerate opposite-parity band structures with connecting $E3$ matrix elements. Such parity doublet bands are the signature of octupole deformation in odd-mass nuclei. The experimental signatures of the octupole interaction are the collective $E3$ transition rates and the enhanced $E1$ transition rates between the opposite-parity states. Experimental data of the $B(E3)$ transition rates are scarce as these are very difficult to access experimentally.

Enhanced $E1$ transitions also manifest the presence of low-lying octupole vibrational states in well-deformed reflection-symmetric nuclei [6]. Measurement of the transi-

*subhphy@gmail.com

[†]Present address: Extreme Light Infrastructure - Nuclear Physics, Horia Hulubei National Institute for R&D in Physics and Nuclear Engineering, Bucharest-Magurele, 077125, Romania.

tion strength can play a crucial role in addressing whether the nucleus of interest has strong octupole correlations to produce an octupole-deformed shape or not. Indeed, the $B(E1)$ transition strengths between the opposite-parity bands have been observed for several nuclei, viz., ^{144}Ba [7], ^{224}Ra [4], and ^{228}Th [8] of the nuclear chart. Enhanced $E3$ matrix elements for the stable octupole-deformed band in $^{222,224,226}\text{Ra}$ nuclei have been reported in the literature [9]. The magnitude of the electric dipole moment shows significant variation with mass and is nearly zero for ^{224}Ra . In this mass region, the sign of the electric dipole moment changes and this crossing happens at $A = 224$. Similar behavior of the electric dipole moment is reported for the Ba isotopes and the magnitude becomes very small for ^{146}Ba . It is important to note that the shell correction term is responsible for exhibiting the variation of the intrinsic dipole moment [10].

In the $A \approx 80$ mass region, the nuclei with particle (proton or neutron) number 34 ($g_{9/2} \leftrightarrow p_{3/2}$ coupling) tend to incline towards the octupole deformation β_3 [11–13]. The $B(E3; 3_1^- \rightarrow 0_1^+)$ values have been measured in $^{74,76,78,80,82}\text{Se}$ and $^{78,80,82,84,86}\text{Kr}$ nuclei and the $B(E3; 3_1^- \rightarrow 2_1^+)$ values have been measured in the $^{74,76,78,80,82}\text{Se}$ isotopes [14]. Though these values span several orders of magnitude, any connection between the $B(E1)$ and $B(E3)$ transition rates is not obvious. These are the direct indication of octupole collectivity for nuclei in the $A \approx 80$ mass region, while the experimental signals of octupole correlations were reported for ^{78}Br but without transition rate measurements [15]. However, the $E1$ transitions rates between opposite-parity states in ^{73}Br [16], ^{74}Se [17], ^{78}Se [18], ^{80}Kr [19], and ^{82}Kr [20] have been measured, but the conclusive argument on the octupole correlation was missing in these nuclei. Direct measurement of the transition strengths will be essential to probe the nature of octupole correlation in this region.

The γ -ray spectroscopic studies for the low-lying structures of ^{79}Se were reported in Refs. [21–25]. In the present work, we report the enhanced electric dipole strengths, $B(E1)$'s, and the dipole moments, $|D_0|$'s, in ^{79}Se , a first in the $A \sim 80$ mass region, using a detector array of high efficiency. The enhanced $B(E1)$ rates are compared with the theoretical calculations for the bands. The results will probably initiate an open debate of understanding the octupole correlation between the opposite parity states in atomic nuclei.

II. EXPERIMENTAL DETAILS

The fusion-evaporation reaction $^{76}\text{Ge}(^9\text{Be}, \alpha 2n)$ at a beam energy of ≈ 31 MeV was used to study the structure of interest in ^{79}Se (Fig. 1). In this reaction, ^{82}Kr was the most abundant yield, whereas the nucleus of interest, ^{79}Se , was produced as well. The PACE4 calculations [26,27] predict that, for the given target-projectile combination, the population of ^{79}Se peaks at ≈ 36 MeV while that of ^{82}Kr peaks at ≈ 28 MeV. The present beam energy (≈ 31 MeV) was chosen in view of optimally producing both the nuclei for spectroscopic investigation. The ^9Be projectiles obtained from the Pelletron Linac Facility at the Tata Institute of Fundamental Research (TIFR), Mumbai, incident on the mg/cm² thick ^{76}Ge target. The target was centrifuged on a mg/cm² thick lead backing which was posi-

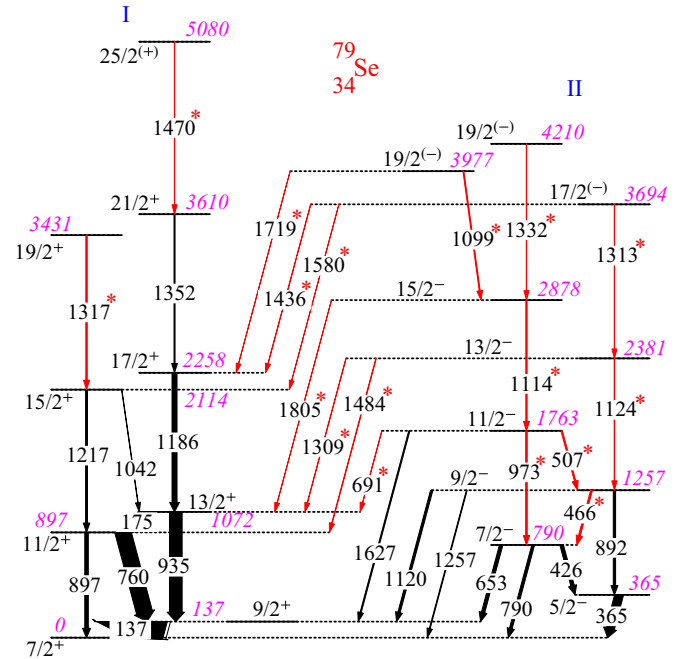


FIG. 1. The partial level structure of ^{79}Se obtained from the present experiment. The red colored transitions, marked by an asterisk, are newly observed γ -ray transitions. The energy of the γ rays and the excited levels are rounded off to the nearest keV. The widths of the arrows are proportional to the intensity of the γ -ray transitions.

tioned to face the beam so as to degrade the beam energy from $E_{\text{lab}} = 37$ MeV to ≈ 31 MeV [28]. The uncertainty of beam energy due to employment of degrader (^{208}Pb) does not affect the velocity of recoiling nuclei ($\beta \approx 0.9\%$) and consequently the level lifetimes obtained from the Doppler-shift attenuation method. The Indian National Gamma Array (INGA), which consisted of 14 Compton-suppressed clover detectors arranged in five different angles 40° , 90° , 115° , 140° , and 157° with respect to the beam axis [29], was employed to detect the deexciting γ rays. Approximately 2.6×10^9 two- and higher-fold γ - γ coincidence time-stamped events were collected and subsequently sorted into different symmetric and angle-dependent E_γ - E_γ matrices and an E_γ - E_γ - E_γ cube using the MARCOS program [29] developed at TIFR, Mumbai. The matrices and the cube were analyzed using the INGASORT [30] and RADWARE [31,32] software packages. The multipolarities and the electromagnetic characters of the observed γ -ray transitions were determined from the measurements of the ratio for directional correlation from oriented state (R_{DCO}) [33,34], the angular distribution from oriented nuclei (ADO) ratio (R_θ) [35], the linear polarization asymmetry (A) [36–39], and the mixing ratio (δ) [40,41]. The experimental details and data analysis procedures are described in detail in Refs. [42,43].

In the present investigation, the detectors at 157° and 90° with respect to the beam direction were used to evaluate the R_{DCO} values, which have been compared with the theoretical DCO ratios [33,34] for multipolarity assignments of the γ -ray transitions. The DCO ratio for a γ transition (γ_1) at an angle of $\theta_1 = 157^\circ$ with respect to another transition (γ_2) at an angle

of $\theta_2 = 90^\circ$ is extracted using the relation

$$R_{\text{DCO}} = \frac{I_{\gamma_1}(\text{At } 157^\circ; \text{Gated by } \gamma_2 \text{ at } 90^\circ)}{I_{\gamma_1}(\text{At } 90^\circ; \text{Gated by } \gamma_2 \text{ at } 157^\circ)}. \quad (1)$$

For this purpose, an asymmetric matrix was constructed with γ -ray events detected at 157° on one axis and coincident events from 90° were placed on the other axis. Theoretically, for a stretched transition, the R_{DCO} should be close to unity if the gating transition has the same multipolarity as that of the observed (analyzed) transition. The DCO ratios for a stretched dipole (quadrupole) transition gated by a pure quadrupole (dipole) transition are ≈ 0.5 (2.0).

For a mixed transition, the R_{DCO} value depends on the detector angles, the mixing ratio (δ), and the width of the substate population (σ/j) of the reaction. To evaluate δ for a mixed transition from the measured DCO ratio $\sigma/j = 0.35$ has been used for the calculations. The DCO ratios were evaluated using the gate on a transition of known multipolarity and δ values. The gate width was set sufficiently narrow to eliminate or minimize contamination. The DCO ratios were then compared with the values calculated using ANGCor [44] with the δ value being varied as a parameter, to check for the best agreement.

The ADO ratio for a γ transition (γ_1) has been obtained from the relation

$$R_\theta = \frac{I_{\gamma_1}(\text{Measured at } \theta_1 = 157^\circ; \text{Gated by all})}{I_{\gamma_1}(\text{Measured at } \theta_2 = 90^\circ; \text{Gated by all})}. \quad (2)$$

Here I_{γ_1} (Measured at θ_1 (θ_2) = 157° (90°); Gated by all) corresponds to the γ -ray coincidence intensity observed by the detectors at an angle θ_1 (θ_2) by setting gates on the detectors at all other angles. For this purpose, two asymmetric matrices were constructed. The first one consisted of events with γ rays detected at 157° on one axis and coincident events from any other angle were placed on the other axis. The other matrix was similar to the first one except that the γ rays detected at 90° were placed on one axis instead of at 157° . Typical R_θ values were 0.6 (1.6) for the stretched dipole (quadrupole) γ -ray transitions; however, R_θ differs for the mixed transitions. The values for the stretched transitions were determined from the transitions of known multipolarity in ^{82}Kr [20].

The clover detectors at 90° of INGA were used for the measurement of the A 's which provide useful information regarding the definitive assignment of the spin-parity of the excited states. Two asymmetric E_γ - E_γ matrices were constructed with the horizontally (N_\parallel) or vertically (N_\perp) scattered γ rays with respect to the reference plane (containing both the beam axis and the emission direction of the γ ray) at 90° detectors on one axis and the coincident γ -ray events from all other detectors on the second axis. The value of A [36–39] is the function of N_\parallel , N_\perp , and the energy of the γ transition (E_γ), which can be expressed as

$$A(E_\gamma) = \frac{a(E_\gamma)N_\perp - N_\parallel}{a(E_\gamma)N_\perp + N_\parallel}. \quad (3)$$

Here, the asymmetry correction factor $a(E_\gamma) = N_\parallel/N_\perp$ represents the geometrical asymmetry of the detection system

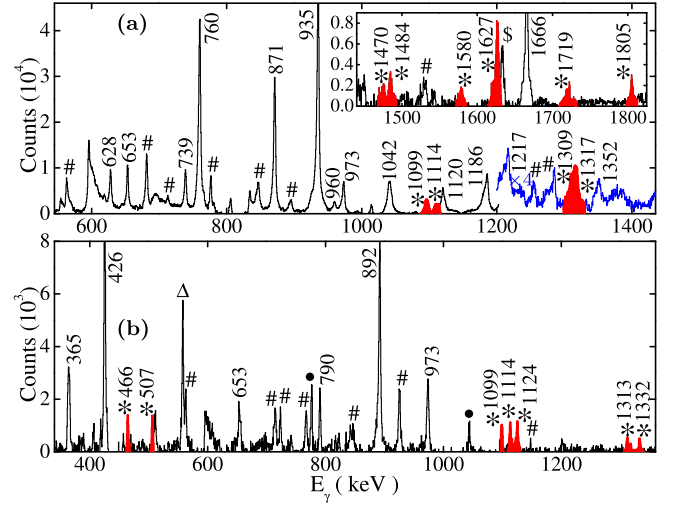


FIG. 2. Experimental spectra created by (a) the gate on the 137.1-keV transition and (b) the sum gate on 365.0- and 973.1-keV transitions show the peaks (rounded off to the nearest keV) in ^{79}Se . The peaks marked by “#” represent the transitions belonging to the structures (not shown in Fig. 1) other than bands I and II. The newly observed peaks are marked by asterisks and filled by red (gray). The spectrum shown in the inset of panel (a) is constructed from the sum gate of 137.1-, 935.4-, and 1186.0-keV transitions. Peaks from the ^{20}Ne , ^{77}As , and ^{82}Kr nuclei have been marked with “\$,” “•,” and “ Δ ,” respectively. The region after 1200 keV of the spectrum (colored by blue) has been multiplied by 4 to increase visibility of the peaks.

(INGA) that has been determined by the unpolarized radioactive ^{152}Eu and ^{133}Ba sources and found to be close to unity [1.02(1)]. For the $\Delta I = 1$ and $\Delta I = 2$ transitions, the positive, negative, and near-zero A values were expected for the γ -ray transitions of electric, magnetic, and mixed character, respectively. For the $\Delta I = 0$ transitions, the sign of the polarization value varies with the $\delta(E2/M1)$ values of the γ -ray transition. The value of A follows the same trend as that of the polarization value. The positive and negative A values are indicative of their magnetic and electric character up to $\delta \approx 0.7$, above which the multipolarity is the same as for stretched transitions, i.e., negative for magnetic and positive for electric.

III. EXPERIMENTAL RESULTS

The proposed structure of ^{79}Se obtained in the present investigation is shown in Fig. 1, with 2 bands, bands I (positive-parity) and II (negative-parity), as well as 13 interband (parity changing) transitions. Seventeen γ transitions and eight levels have been newly observed in the previously reported level structure of ^{79}Se [21,25]. Table I shows the γ energies (E_γ), relative intensities (I_γ), R_{DCO} , R_θ , A , δ , and assigned spin-parities of the states of ^{79}Se . Figure 2 shows sample spectra supporting the present level scheme. The excited states in band I, built on the $\nu g_{9/2}$ orbital, have been reported in Refs. [21,25] with spin-parity values firmly assigned up to $17/2^+$. We confirmed the previously reported structures of band I and extended it up to the 5080-keV excited state through the placement of the 1317.0-keV ($19/2^+ \rightarrow 15/2^+$)

TABLE I. γ energy (E_γ), relative intensity (I_γ), R_{DCO} , R_θ , linear polarization asymmetry (A), mixing ratio (δ), and assignment of the γ transitions in ^{79}Se . Intensities of γ rays are normalized to the 137.1-keV transition, with $I_\gamma = 1000.0$.

Energy (E_x)	γ energy (E_γ)	$J_i^\pi \rightarrow J_f^\pi$	Intensity (I_γ)	DCO ratio (R_{DCO})	Anisotropy (R_θ)	Asymmetry (A)	Mixing ratio (δ)	$\sigma\lambda$
Band I								
137.1	137.1(2)	$9/2^+ \rightarrow 7/2^+$	1000.0(52)	0.75(6) ^a	1.06(7)			M1+E2
897.4	760.2(4)	$11/2^+ \rightarrow 9/2^+$	229.5(38)		0.65(6)	-0.03(1)		M1+E2
	897.4(5)	$11/2^+ \rightarrow 7/2^+$	89.5(38)		1.87(16)	+0.20(11)		E2
1072.5	175.1(2)	$13/2^+ \rightarrow 11/2^+$	2.6(8)	0.61(6) ^a	0.74(11)		+0.10(4)	M1+E2
	935.4(6)	$13/2^+ \rightarrow 9/2^+$	181.6(8)	0.93(8) ^a	1.54(13)	+0.10(2)		E2
2114.3	1041.9(7)	$15/2^+ \rightarrow 13/2^+$	9.8(6)	0.59(5) ^a	0.61(7)	+0.02(3)	+0.06(3)	M1+E2
	1216.8(7)	$15/2^+ \rightarrow 11/2^+$	26.8(6)	0.97(8) ^a	1.69(15)	+0.08(6)		E2
2258.4	1186.0(6)	$17/2^+ \rightarrow 13/2^+$	71.0(23)	1.05(9) ^a	1.60(14)	+0.11(8)		E2
3431.3	1317.0(7)	$19/2^+ \rightarrow 15/2^+$	20.5(25)		1.65(14)	+0.10(7)		E2
3610.4	1352.0(7)	$21/2^+ \rightarrow 17/2^+$	14.5(17)	0.95(11) ^a	1.61(18)	+0.17(8)		E2
5080.4	1470.2(9)	$25/2^{(+)} \rightarrow 21/2^+$	6.8(13)		1.76(19)			(E2)
Band II								
365.0	365.0(2)	$5/2^- \rightarrow 7/2^+$	123.2(21)		0.94(8)	+0.22(12)		E1
790.5	425.6(3)	$7/2^- \rightarrow 5/2^-$	21.5(12)	1.21(14) ^b	2.04(26)	-0.09(4)	+0.21(6)	M1+E2
	653.3(4)	$7/2^- \rightarrow 9/2^+$	47.5(12)	0.54(5) ^a	0.95(9)	+0.08(5)		E1
	790.4(5)	$7/2^- \rightarrow 7/2^+$	38.5(12)	0.94(8) ^a	1.49(12)	+0.14(17)		E1
1256.9	466.0(5)	$9/2^- \rightarrow 7/2^-$	11.0(17)		0.66(10)			M1+E2
	892.0(5)	$9/2^- \rightarrow 5/2^-$	34.1(17)		1.43(12)	+0.10(3)		E2
	1120.1(6)	$9/2^- \rightarrow 9/2^+$	20.2(17)		1.46(13)	-0.10(6)		E1
	1257.0(6)	$9/2^- \rightarrow 7/2^+$	24.8(17)		0.59(5)			E1
1763.7	507.0(5)	$11/2^- \rightarrow 9/2^-$	6.2(14)		0.57(9)			M1+E2
	973.1(5)	$11/2^- \rightarrow 7/2^-$	21.3(14)	0.92(10) ^a	1.64(15)	+0.08(5)		E2
	691.0(9)	$11/2^- \rightarrow 13/2^+$	1.1(2)		0.87(12)			E1
	1626.6(8)	$11/2^- \rightarrow 9/2^+$	16.1(14)	0.58(6) ^a	0.67(7)	+0.07(4)		E1
2381.4	1124.0(7)	$13/2^- \rightarrow 9/2^-$	9.5(8)	0.97(10) ^a	1.68(19)	+0.15(9)		E2
	1309.0(11)	$13/2^- \rightarrow 13/2^+$	4.5(8)	1.07(15) ^a	1.56(18)			E1
	1484.3(8)	$13/2^- \rightarrow 11/2^+$	4.9(8)		0.52(7)	+0.07(8)		E1
2878.0	1114.3(6)	$15/2^- \rightarrow 11/2^-$	15.0(6)	1.02(9) ^a	1.69(18)	+0.16(9)		E2
	1805.4(8)	$15/2^- \rightarrow 13/2^+$	5.0(6)	0.58(8) ^a	0.67(9)	+0.07(8)		(E1)
3694.5	1313.0(6)	$17/2^{(-)} \rightarrow 13/2^-$	6.1(5)		1.54(21)			(E2)
	1436.0(11)	$17/2^{(-)} \rightarrow 17/2^+$	1.6(5)		1.34(16)			(E1)
	1580.4(13)	$17/2^{(-)} \rightarrow 15/2^+$	0.8(5)		0.64(8)			(E1)
4210.0	1332.0(7)	$19/2^{(-)} \rightarrow 15/2^-$	4.5(9)		1.48(12)			(E2)
3977.1	1098.7(7) ^c	$19/2^{(-)} \rightarrow 15/2^-$	14.4(9)	1.21(14) ^a	1.78(21)			(E2)
	1719.0(9)	$19/2^{(-)} \rightarrow 17/2^+$	1.5(4)	0.61(8) ^a	0.59(7)			(E1)

^aDCO ratios are obtained from stretched electric quadrupole ($E2$) transitions.

^bDCO ratios are obtained from stretched electric dipole ($E1$) transitions.

^cNot a member of band II.

and 1470-keV ($25/2^{(+)} \rightarrow 21/2^+$) transitions. Zell *et al.* [21] had reported the 364.9-, 790.3-, and 1256.8-keV excited states having spin-parities $5/2^-$, ($7/2^-$, $9/2^-$), and ($5/2^+$, $9/2^-$), respectively, as nonband levels. In a later study by Singh *et al.* [23], the 790.3-keV state was tentatively assigned a spin-parity of ($7/2^-$) and the 1256-keV level was tentatively identified as ($9/2^-$). Measured R_{DCO} , R_θ , and A values of the 425.6 and 653.3-keV transitions showed their $M1 + E2$ and $E1$ characters, respectively, confirming the spin-parity of the 790.3-keV excited state as $7/2^-$. The R_θ and A values of the 892.0-keV transition are indicating of its $E2$ behavior which leads to the spin-parity of $9/2^-$ for the 1256.8-keV excited state. We have rearranged these negative-parity states as members of band II along with the placement of 7 new in-band γ -ray transitions as depicted in Fig. 1. We have observed 8

new parity changing transitions connecting band II to band I. Measured R_{DCO} values of the 1626.6, 1805.4, and 1719.0-keV γ rays showed their dipole character, while 1309.0- and 1436.0-keV transitions indicate the $\Delta I = 0$ $E1$ nature. R_{DCO} values for the 691.0-, 1484.3-, and 1580.4-keV transitions remain undetermined and lead to the tentative $E1$ assignment to these γ transitions. The A value for the 790.4-, 1484.3-, and 1805.4-keV γ -ray transitions overlap zero values within the uncertainties (Table I) and make $E1$ assignments tentative for these γ rays. The remaining connecting transitions were too weak to extract their A values.

A. Line shape analysis

The level lifetimes of the six levels ($21/2^+$ to $11/2^+$) of band I and the four states ($7/2^-$, $9/2^-$, $11/2^-$, and $15/2^-$)

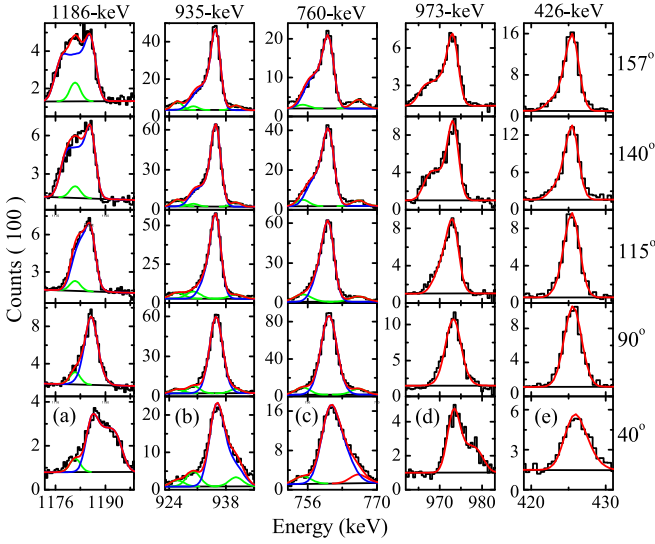


FIG. 3. The experimental spectra along with the fitted line shapes for the γ transitions (a) 1186.0, (b) 935.4, (c) 760.2 (d) 973.1, and (e) 425.6-keV of the bands I and II in ^{79}Se . The desired line shapes of γ transitions, contaminant peaks, and total line shapes are represented by the blue, green, and red curves, respectively.

of band II in the ^{79}Se nucleus have been extracted using the combination of developments described in Ref. [45] and the LINESHAPE package [46,47]. Here experimental Doppler-broadened shapes of the γ -ray transitions are analyzed to obtain the lifetime. The energy loss and the trajectories of the residual nuclei (^{79}Se) inside the target were simulated using Monte Carlo techniques with the updated stopping powers from the SRIM database [42,43,48]. The 1317.0-keV ($19/2^+ \rightarrow 15/2^+$) and 1352.0-keV ($21/2^+ \rightarrow 17/2^+$) transitions of band I and the 1114.3-keV ($15/2^- \rightarrow 11/2^-$) transition of band II were the highest transitions, respectively, for which the effective lifetimes of <0.5 ps, <0.3 ps, and <0.4 ps, respectively, have been extracted from the present analysis. Sequential line-shape fitting gives the level lifetime of the lower-lying states of the cascade. The side-feeding contribution to the level lifetime has been modeled with a cascade of five transitions whose moment of inertia is similar to the band of interest. Variation in the side-feeding intensity resulted in a change of the evaluated level lifetime by less than 10%.

The observed Doppler-broadened shape in the experimental spectra has been fitted simultaneously at five different angles of 40° , 90° , 115° , 140° , and 157° to obtain the lifetime of the states as illustrated in Fig. 3. The extracted level lifetimes and the corresponding reduced transition probabilities [$B(M1)$, $B(E1)$, and $B(E2)$ values] for bands I and II are recorded in Table II. The lifetimes obtained in the present work are in good agreement with the values reported in Refs. [22,23]. The uncertainties on the lifetimes, derived from the χ^2 -minimization analysis, do not include the systematic contribution of the stopping powers from the SRIM database, which is expected to be $\approx 5\%$.

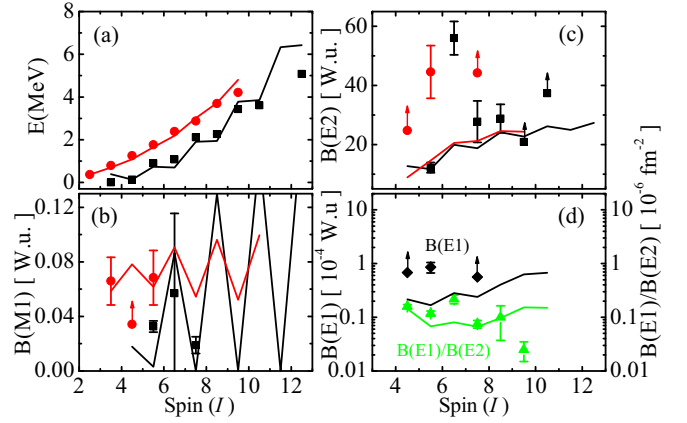


FIG. 4. Panels (a), (b), and (c) show the comparison of the experimental energies, $B(M1)$ and $B(E2)$ values, respectively, for bands I (solid square) and II (solid circle) in ^{79}Se with the RAT-PRM calculations. The solid black and red (gray) lines represent the RAT-PRM calculations for bands I and II, respectively. In panel (d), the comparison of the measured $B(E1)$ (solid black diamond) and $B(E1)/B(E2)$ [green (light gray) up-triangle] values for $I \rightarrow I - 1$ with the RAT-PRM calculations represented by the solid black and green (light gray) lines, respectively.

IV. DISCUSSION

The positive-parity band I and the negative-parity band II have experimental features (cf. Fig. 4) similar to the bands based on $\nu g_{9/2}$ and $\nu f_{5/2}$ orbitals, respectively, observed in the neighboring ^{77}Se [49], $^{79,81}\text{Kr}$ [50,51], ^{81}Sr [52], and ^{83}Zr [53,54] nuclei. Li *et al.* [25] had reported the origin of the collective structure in band I in ^{79}Se was based on the $g_{9/2}$ orbital.

One of the most striking features of the level scheme of ^{79}Se is the observation of the strong $E1$ transitions with large $B(E1)/B(E2)$ ratios ($\approx 0.1 \times 10^{-6} \text{ fm}^{-2}$) and $B(E1)$ ($\approx 10^{-4}$ W.u.) transition rates [Figs. 4(d) and 5(a) and Table II]. Such large transition rates are comparable to the values observed in the opposite-parity (octupole) bands of ^{142}Eu [55], $^{124,125}\text{Ba}$ [56], ^{117}Xe [57], and ^{124}Cs [58]. Figure 5(a) shows that the $B(E1)/B(E2)$ values of ^{79}Se are merged with octupole-correlated bands of neighboring ^{78}Br [15] but not in agreement with the octupole-deformed bands of ^{144}Ba [59] and ^{224}Th [60]. Thus, bands I and II, connected through the parity-changing transitions, indicate the existence of octupole correlation in ^{79}Se .

The feasibility of the observed octupole correlations in ^{79}Se has been checked by adopting the relativistic density functional theory [61]. The covariant density functional theory (CDFT) has been developed in three-dimensional (3D) lattice space to describe nuclei without any symmetric restriction [62,63], such as exotic nuclear linear-chain [63] and toroidal states [64]. For the present purpose, the potential energy surface in the β_{20} - β_{30} plane is calculated by the CDFT in a 3D lattice with the successful density functional PC-PK1 [65] (Fig. 6). The potential energy surface is very soft with respect to the shape degree of freedom β_{30} , which further upholds the propositions of octupole correlations in ^{79}Se .

TABLE II. Measured transition energies (E_γ), branching ratios (Br), level lifetimes (τ), $B(M1)$, $B(E1)$, $B(E2)$, and the electric quadrupole and dipole moments, $|Q_0|$ and $|D_0|$ values, of bands I and II in ^{79}Se . The upward and downward arrows represent lower and upper limits of the measured values, respectively. The transition has been considered as pure dipole ($M1$) in the $B(M1)$ calculations if a mixing ratio of the respective transition is not provided in Table I.

	J_i (\hbar)	E_γ (keV)	$\sigma\lambda$	Br (%)	τ^a (ps)	τ^b (ps)	$B(M1)$ (10^{-3} W.u.)	$B(E2)$ (W.u.)	$B(E1)$ (10^{-4} W.u.)	Moment
Band I										
897.4	11/2 ⁺	760.2	$M1 + E2$	72(2)	$0.9^{+0.2}_{-0.1}$	1.6 ± 0.2	32.6 ± 4.2			
		897.4	$E2$	28(2)				12.2 ± 1.8		3.2 ± 0.5^c
1072.5	13/2 ⁺	175.1	$M1 + E2$	1.4(5)	$1.2^{+0.4}_{-0.3}$	1.0 ± 0.1	82.2 ± 33.8	34.1 ± 14.0		
		935.4	$E2$	98.6(5)				55.8 ± 5.6		2.3 ± 0.3^c
2114.3	15/2 ⁺	1041.9	$M1 + E2$	27(3)	$0.6^{+0.4}_{-0.2}$	0.4 ± 0.1	18.9 ± 6.1	0.08 ± 0.03		
		1216.8	$E2$	73(3)				27.7 ± 7.0		2.1 ± 0.3^c
2258.4	17/2 ⁺	1186.0	$E2$	100	$1.0^{+0.5}_{-0.4}$	0.6 ± 0.1		28.8 ± 4.8		1.8 ± 0.2^c
3431.3	19/2 ⁺	1317.0	$E2$	100		$0.5\downarrow$		$20.5\uparrow$		$1.3\uparrow^c$
3610.4	21/2 ⁺	1352.0	$E2$	100		$0.3\downarrow$		$29.9\uparrow$		$1.6\uparrow^c$
Band II										
365.0	5/2 ⁻	365.0	$E1$	100	135 ± 35				0.8 ± 0.2	4.0 ± 1.0^d
790.5	7/2 ⁻	425.6	$M1 + E2$	20(2)	$1.7^{+0.5e}_{-0.3}$	1.2 ± 0.2	65.9 ± 17.5	20.4 ± 5.4		
		653.3 ^e	$E1$	44(2)					$7.0\downarrow$	$9.4\downarrow^d$
		790.4 ^f	$E1$	36(2)					$3.2\downarrow$	$6.4\downarrow^d$
1256.9	9/2 ⁻	466.0	$M1 + E2$	12(2)	$1.0^{+0.5}_{-0.4}$	$1.1\downarrow$	$34.3\uparrow$			
		892.0	$E2$	38(2)				$24.8\uparrow$		$2.3\uparrow^c$
		1120.1	$E1$	22(2)					$0.8\uparrow$	$3.9\uparrow^d$
		1257.0	$E1$	28(2)					$0.7\uparrow$	$3.3\uparrow^d$
1763.7	11/2 ⁻	507.0	$M1 + E2$	14(3)	$1.2^{+0.6}_{-0.4}$	0.5 ± 0.1	68.4 ± 20.0			
		973.1	$E2$	48(3)				44.6 ± 8.9		2.3 ± 0.4^c
		691.0	$E1$	3(1)					1.0 ± 0.4	3.2 ± 1.3^d
		1626.6	$E1$	35(3)					0.9 ± 0.2	3.4 ± 0.8^d
2878.0	15/2 ⁻	1114.3	($E2$)	75(3)		$0.4\downarrow$		$40.2\uparrow$		$1.6\uparrow^c$
		1805.4	($E1$)	25(3)					$0.6\uparrow$	$2.6\uparrow^d$

^aLifetimes from previous measurements [22,23].

^bLifetimes from present measurements.

^cElectric quadrupole moment (Q_0) in e b.

^dElectric dipole moment (D_0) in 10^{-2} e fm.

^eLifetime from Ref. [24].

^fUpper limit of the $B(E1)$ transition strength and the $|D_0|$ value has been calculated considering zero mixing $\delta(M2/E1) = 0$.

The origin of the $E1$ transitions between the opposite-parity bands I and II in the ^{79}Se nucleus has been investigated by comparing the measured values with the reflection-asymmetric triaxial particle rotor model (RAT-PRM) calculations [66,67]. The reflection-asymmetric particle rotor model is used to study nuclear chirality [68] and multiple chiral doublet bands [15,67,69,70]. Figure 4 shows the comparisons of the experimental energy, $B(M1)$, $B(E2)$, and $B(E1)$ values in ^{79}Se with the RAT-PRM calculations. Here, a reflection-asymmetric potential is included in the particle rotor Hamiltonian so that the positive- and negative-parity states simultaneously appear in the calculations [66]. The CDFT calculation in 3D lattice space gives the quadrupole deformation parameters $\beta_{20} = 0.19$ and $\gamma = 0^\circ$ and the octupole parameter $\beta_{30} = 0$. As the potential energy surface is soft for β_{30} , $\beta_{30} = 0.03$ is adopted to include the effect of octupole correlations in the RAT-PRM calculations. The calculated energy is normalized to coincide with the experimental energy at $I = 9/2\hbar$ for positive-parity band I and $I = 7/2\hbar$ for negative-parity band II. As shown in Fig. 4(a), the calculated excitation energies reproduce the experimental

data well. Variation of $B(M1)$ and $B(E2)$ values with spin is in good agreement though the magnitudes of the experimental $B(E2)$ values are a bit underestimated. Figure 4(d) shows the comparison of experimental $B(E1)$ and $B(E1)/B(E2)$ values with the RAT-PRM calculation. It confirms not only the β_{30} deformation parameter suggested by the CDFT but also the configuration assignments for bands II (mainly dominated by $\nu f_{5/2}[\Omega = 5/2]$) and I (mainly dominated by $\nu g_{9/2}[\Omega = 5/2]$) as well as the octupole correlations between them. Thus, the present investigation suggests that the octupole interaction potential in the two opposite-parity bands exists in ^{79}Se .

The present investigation also exhibits the existence of the strongly enhanced $E1$ transitions between the opposite-parity bands. Indeed, the calculated $B(E1)$ and $B(E1)/B(E2)$ values with $\beta_{30} = 0.03$ adopted in the present RAT-PRM satisfactorily agree with the experimental data. The large $B(E1)$ strengths are indicative of the existence of a permanent electric dipole in ^{79}Se . The electric dipole moment $|D_0|$ can be calculated directly from the measured $B(E1)$ rates according to the formula $B(E1 : I_i \rightarrow I_f) = \frac{3}{4\pi} D_0^2 \langle I_i K_i | 10 | I_f K_f \rangle^2$,

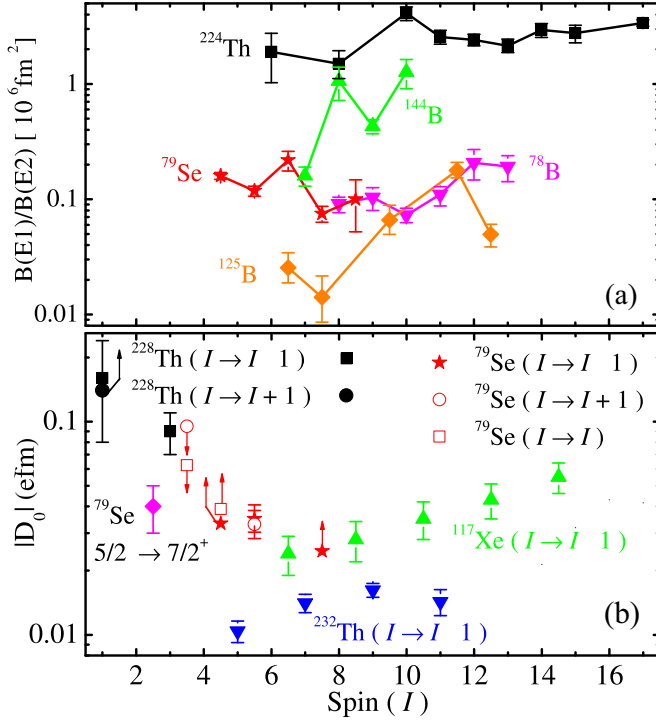


FIG. 5. (a) The experimental $B(E1 : I \rightarrow I - 1)/B(E2 : I \rightarrow I - 2)$ ratios for band II in ^{79}Se compared with ^{78}Br [15], $^{125,144}\text{Ba}$ [56,59], and ^{224}Th [60]. (b) The $|D_0|$ values extracted from the $B(E1)$ rates of $I \rightarrow I - 1$, $I \rightarrow I + 1$, and $I \rightarrow I$ states in ^{79}Se compared with ^{117}Xe [57] and $^{228,232}\text{Th}$ [8,60]. The $|D_0|$ value of the $5/2^-$ state is extracted using the lifetime reported in Ref. [22].

where $\langle I_i K_i 10 | I_f K_f \rangle$ is the Clebsch-Gordan coefficient and $K_i = K_f = 5/2$.

Figure 5(b) shows that the extracted $|D_0|$ values are similar to the octupole vibrational and correlational bands of ^{117}Xe [57] and ^{232}Th [60]. This unambiguously suggests that the octupole correlation exists in ^{79}Se .

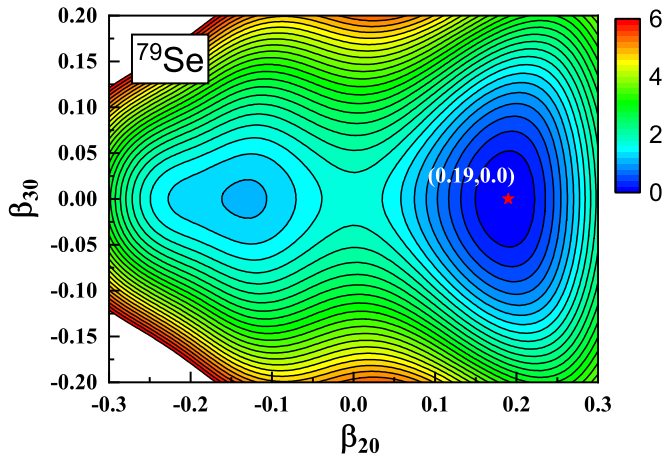


FIG. 6. The potential energy surface of ^{79}Se calculated by the CDFT in the 3D lattice approach [63]. The contour separation is 0.2 MeV. The pentagram corresponds to the point of the minimum energy.

Measured $B(E1)$ rates result in a large value of $|D_0| = 9.4 \times 10^{-2} \downarrow e \text{ fm}$ for the $7/2^-$ state, calculated from the 653.3-keV transition, as depicted in Fig. 5(b). This figure shows that the extracted $|D_0|$ value is the same order of magnitude as the octupole deformed bands in ^{228}Th [8]. To understand the intrinsic character of the $7/2^-$ state, a systematic investigation on the low-lying states of the nuclei in this mass region is warranted. Such work will also help us to constrain suitable candidates for experimental studies of atomic electric-dipole moments that might reveal extensions to the standard model.

The successful interpretation of the experimental results in the framework of the RAT-PRM calculation indicates that bands I and II in ^{79}Se are generated by the octupole correlation due to the availability of the valence nucleons in the $g_{9/2}-(f_{5/2}/p_{3/2,1/2})$ orbitals near the Fermi surface.

V. SUMMARY

We have observed the interconnecting $E1$ transitions in the two opposite-parity bands I and II. Measured energies and transition rates [$B(M1)$, $B(E2)$, $B(E1)$, and $B(E1)/B(E2)$ values] of the bands are in good agreement with the RAT-PRM calculations. The calculations indicate an octupole correlation in ^{79}Se due to the availability of valence nucleons (neutrons) in the $g_{9/2}-(f_{5/2}/p_{3/2,1/2})$ orbitals near the Fermi surface. Thus, the present work on ^{79}Se is the first conclusive experimental evidence of octupole correlation arising due to the neutrons in the $g_{9/2}-(f_{5/2}/p_{3/2,1/2})$ orbitals. The uniqueness of the present work is the observation of the enhanced $B(E1)$ strength and the corresponding $|D_0|$ values. The $|D_0|$ values for the $7/2^-$ state are the same order of magnitude as the octupole-deformed bands in ^{228}Th [8]. These results facilitate a more comprehensive understanding of the nuclear many-body system. It may contribute to developing a unified microscopic theory of the octupole correlation in atomic nuclei.

ACKNOWLEDGMENTS

We acknowledge the help and support from the INGA collaboration. We thank Prof. S. Chattopadhyay (SINP) for providing the target material. The authors remain grateful to Professor S. Q. Zhang for fruitful discussions. We are thankful to the staff at the Pelletron LINAC Facility in TIFR for their efforts in delivering steady and uninterrupted ^9Be beam. This work is supported by the Department of Atomic Energy, Government of India (Project Identification Code: 12-R&DTFR-5.02-0200), and the Department of Science and Technology, Government of India (Grant No. IR/S2/PF-03/2003-II). The authors gratefully acknowledge the financial support by the Department of Science and Technology (DST) for the INGA project (Grant No. IR/S2/PF-03/2003-II). H.P. is grateful for the support of the Ramanujan Fellowship research grant under SERB-DST (Grant No. SB/S2/RJN-031/2016). S.R. would like to acknowledge the financial assistance from the UGC-DAE Consortium for Scientific Research, Kolkata Centre, un-

der the Collaborative Research Scheme (CRS) (Grant No. UGC-DAE-CSR/KC/CRS/19/NP13/0924) and the FRPDF grant of Presidency University, Kolkata, India. S.R. is also grateful to the SERB-DST for financial support under core research grants (File Number: CRG/2020/003370). S. Bhattacharya would like to acknowledge financial assistance from the UGC-DAE-CSR project (Grant No. UGC-DAE-CSR-KC/CRS/19/NP04/0915) and the IUAC project (Grant No. IUAC/XIII.3A/UFR-55313). The work of Q.B.C. is supported by the Deutsche Forschungsgemeinschaft (DFG) and the National Natural Science Foundation of China (NSFC)

through funds provided to the Sino-German CRC 110 “Symmetries and the Emergence of Structure in QCD” (DFG Grant No. TRR110 and NSFC Grant No. 12070131001). Y.Y.W., Z.X.R., and J.M. would like to acknowledge the support of the National Natural Science Foundation of China (Grants No. 11935003 and No. 12070131001), the National Key R&D Program of China (Contracts No. 2018YFA0404400 and No. 2017YFE0116700), the State Key Laboratory of Nuclear Physics and Technology, Peking University (Grant No. NPT2020ZZ01), and the China Postdoctoral Science Foundation under Grants No. 2020M670014 and No. 2020M670013.

-
- [1] A. Bohr and B. R. Mottelson, *Nuclear Structure* (Benjamin, New York, 1975), Vol. II.
- [2] S. Frauendorf, *Rev. Mod. Phys.* **73**, 463 (2001).
- [3] P. A. Butler and W. Nazarewicz, *Rev. Mod. Phys.* **68**, 349 (1996).
- [4] L. P. Gaffney *et al.*, *Nature (London)* **497**, 199 (2013).
- [5] J. Dobaczewski, J. Engel, M. Kortelainen, and P. Becker, *Phys. Rev. Lett.* **121**, 232501 (2018).
- [6] A. V. Afanasjev and S. Mizutori, *Z. Phys. A* **353**, 267 (1995).
- [7] B. Bucher, S. Zhu, C. Y. Wu, R. V. F. Janssens, D. Cline, A. B. Hayes, M. Albers, A. D. Ayangeakaa, P. A. Butler, C. M. Campbell, M. P. Carpenter, C. J. Chiara, J. A. Clark, H. L. Crawford, M. Cromaz, H. M. David, C. Dickerson, E. T. Gregor, J. Harker, C. R. Hoffman *et al.*, *Phys. Rev. Lett.* **116**, 112503 (2016).
- [8] M. M. R. Chishti *et al.*, *Nat. Phys.* **16**, 853 (2020).
- [9] P. A. Butler, *J. Phys. G: Nucl. Part. Phys.* **43**, 073002 (2016).
- [10] P. A. Butler and W. Nazarewicz, *Nucl. Phys. A* **533**, 249 (1991).
- [11] R. B. Piercey, A. V. Ramayya, R. M. Ronningen, J. H. Hamilton, V. Maruhn-Rezwani, R. L. Robinson, and H. J. Kim, *Phys. Rev. C* **19**, 1344 (1979).
- [12] M. S. Kaplan *et al.*, *Phys. Lett. B* **215**, 251 (1988).
- [13] P. D. Cottle, *Phys. Rev. C* **41**, 517 (1990).
- [14] T. Kibédi and R. H. Spear, *At. Data Nucl. Data Tables* **80**, 35 (2002).
- [15] C. Liu, S. Y. Wang, R. A. Bark, S. Q. Zhang, J. Meng, B. Qi, P. Jones, S. M. Wyngaardt, J. Zhao, C. Xu, S. G. Zhou, S. Wang, D. P. Sun, L. Liu, Z. Q. Li, N. B. Zhang, H. Jia, X. Q. Li, H. Hua, Q. B. Chen *et al.*, *Phys. Rev. Lett.* **116**, 112501 (2016).
- [16] S. Bhattacharya, T. Trivedi, D. Negi, R. P. Singh, S. Muralithar, R. Palit, I. Ragnarsson, S. Nag, S. Rajbanshi, M. K. Raju, V. V. Parkar, G. Mohanto, S. Kumar, D. Choudhury, R. Kumar, R. K. Bhowmik, S. C. Pancholi, and A. K. Jain, *Phys. Rev. C* **100**, 014315 (2019).
- [17] J. Adam *et al.*, *Z. Phys. A* **332**, 143 (1989).
- [18] R. Schwengner *et al.*, *Z. Phys. A* **326**, 287 (1987).
- [19] L. Funke *et al.*, *Nucl. Phys. A* **355**, 228 (1981).
- [20] P. Kemnitz *et al.*, *Nucl. Phys. A* **425**, 493 (1984).
- [21] K. O. Zell *et al.*, *Z. Phys. A* **292**, 135 (1979).
- [22] M. F. Kudoyarov *et al.*, 41st Conf. Nucl. Spectroscopy Nucl. Struct., Minsk (1991), p. 59.
- [23] B. Singh, *Nucl. Data Sheets* **135**, 193 (2016).
- [24] M. F. Kudoyarov *et al.*, 38th Conf. Nucl. Spectroscopy Nucl. Struct., Baku (1988), p. 65.
- [25] C. G. Li *et al.*, *Phys. Rev. C* **100**, 044318 (2019).
- [26] A. Gavron, *Phys. Rev. C* **21**, 230 (1980).
- [27] O. B. Tarasov and D. Bazin, *Nucl. Instrum. Methods Phys. Res., Sect. B* **266**, 4657 (2008).
- [28] James F. Ziegler, M. D. Ziegler, and J. P. Biersack, *Nucl. Instrum. Methods Phys. Res., Sect. B* **268**, 1818 (2010).
- [29] R. Palit *et al.*, *Nucl. Instrum. Methods Phys. Res., Sect. A* **680**, 90 (2012).
- [30] R. K. Bhowmik, INGASORT manual (private communication).
- [31] D. C. Radford, *Nucl. Instrum. Methods Phys. Res., Sect. A* **361**, 297 (1995).
- [32] D. C. Radford, *Nucl. Instrum. Methods Phys. Res., Sect. A* **361**, 306 (1995).
- [33] A. Krämer-Flecken *et al.*, *Nucl. Instrum. Methods Phys. Res., Sect. A* **275**, 333 (1989).
- [34] M. K. Kabadiyski, K. P. Lieb, and D. Rudolph, *Nucl. Phys. A* **563**, 301 (1993).
- [35] M. Piiparinen *et al.*, *Nucl. Phys. A* **605**, 191 (1996).
- [36] K. Starosta *et al.*, *Nucl. Instrum. Methods Phys. Res., Sect. A* **423**, 16 (1999).
- [37] Ch. Droste *et al.*, *Nucl. Instrum. Methods Phys. Res., Sect. A* **378**, 518 (1996).
- [38] J. K. Deng *et al.*, *Nucl. Instrum. Methods Phys. Res., Sect. A* **317**, 242 (1992).
- [39] P. M. Jones *et al.*, *Nucl. Instrum. Methods Phys. Res., Sect. A* **362**, 556 (1995).
- [40] T. Yamazaki, *Nucl. Data, Sect. A* **3**, 1 (1967).
- [41] E. D. Mateosion and A. W. Sunyar, *At. Data Nucl. Data Tables* **13**, 391 (1974).
- [42] S. Rajbanshi, A. Bisoi, S. Nag, S. Saha, J. Sethi, T. Trivedi, T. Bhattacharjee, S. Bhattacharyya, S. Chattopadhyay, G. Gangopadhyay, G. Mukherjee, R. Palit, R. Raut, M. S. Sarkar, A. K. Singh, and A. Goswami, *Phys. Rev. C* **89**, 014315 (2014).
- [43] S. Rajbanshi, A. Bisoi, S. Nag, S. Saha, J. Sethi, T. Bhattacharjee, S. Bhattacharyya, S. Chattopadhyay, G. Gangopadhyay, G. Mukherjee, R. Palit, R. Raut, M. S. Sarkar, A. K. Singh, T. Trivedi, and A. Goswami, *Phys. Rev. C* **90**, 024318 (2014).
- [44] E. S. Macias, W. D. Ruhter, D. C. Camp, and R. G. Lanier, *Comput. Phys. Commun.* **11**, 75 (1976).
- [45] S. Das *et al.*, *Nucl. Instrum. Methods Phys. Res., Sect. A* **841**, 17 (2017).
- [46] J. C. Wells and N. R. Johnson, LINESHAPE: A Computer Program for Doppler Broadened Lineshape Analysis, Report No. ORNL-6689, 44, 1991.
- [47] N. R. Johnson, J. C. Wells, Y. Akovali, C. Baktash, R. Bengtsson, M. J. Brinkman, D. M. Cullen, C. J. Gross, H.-

- Q. Jin, I.-Y. Lee, A. O. Macchiavelli, F. K. McGowan, W. T. Milner, and C.-H. Yu, *Phys. Rev. C* **55**, 652 (1997).
- [48] S. Rajbanshi *et al.*, *Phys. Lett. B* **782**, 143 (2018).
- [49] G. D. Johns, J. Doring, R. A. Kaye, G. N. Sylvan, and S. L. Tabor, *Phys. Rev. C* **55**, 660 (1997).
- [50] G. D. Johns, J. Doring, J. W. Holcomb, T. D. Johnson, M. A. Riley, G. N. Sylvan, P. C. Womble, V. A. Wood, and S. L. Tabor, *Phys. Rev. C* **50**, 2786 (1994).
- [51] L. Funke *et al.*, *Nucl. Phys. A* **455**, 206 (1986).
- [52] S. E. Amell *et al.*, *J. Phys. G: Nucl. Phys.* **9**, 1217 (1983).
- [53] D. Rudolph *et al.*, *Z. Phys. A* **338**, 139 (1991).
- [54] W. Fieber *et al.*, *Z. Phys. A* **332**, 363 (1989).
- [55] S. Ali *et al.*, *Phys. Lett. B* **798**, 134960 (2019).
- [56] P. Mason *et al.*, *Phys. Rev. C* **72**, 064315 (2005).
- [57] Z. Liu *et al.*, *Eur. Phys. J. A* **1**, 125 (1998).
- [58] K. Selvakumar, A. K. Singh, C. Ghosh, P. Singh, A. Goswami, R. Raut, A. Mukherjee, U. Datta, P. Datta, S. Roy, G. Gangopadhyay, S. Bhowal, S. Muralithar, R. Kumar, R. P. Singh, and M. K. Raju, *Phys. Rev. C* **92**, 064307 (2015).
- [59] J. H. Hamilton *et al.*, *Acta Phys. Pol., B* **32**, 957 (2001).
- [60] B. Ackermann *et al.*, *Nucl. Phys. A* **559**, 61 (1993).
- [61] *Relativistic Density Functional for Nuclear Structure*, edited by J. Meng, International Review of Nuclear Physics Vol. 10 (World Scientific, Singapore, 2016).
- [62] Z. X. Ren, S. Q. Zhang, and J. Meng, *Phys. Rev. C* **95**, 024313 (2017).
- [63] Z. X. Ren *et al.*, *Sci. China: Phys., Mech. Astron.* **62**, 112062 (2019).
- [64] Z. X. Ren *et al.*, *Nucl. Phys. A* **996**, 121696 (2020).
- [65] P. W. Zhao, Z. P. Li, J. M. Yao, and J. Meng, *Phys. Rev. C* **82**, 054319 (2010).
- [66] Y. Y. Wang, S. Q. Zhang, P. W. Zhao, and J. Meng, *Phys. Lett. B* **792**, 454 (2019).
- [67] Y. P. Wang, Y. Y. Wang, and J. Meng, *Phys. Rev. C* **102**, 024313 (2020).
- [68] S. Frauendorf and J. Meng, *Nucl. Phys. A* **617**, 131 (1997).
- [69] Y. Y. Wang and S. Q. Zhang, *Phys. Rev. C* **102**, 034303 (2020).
- [70] Y. Y. Wang *et al.*, *Sci. Bull.* **65**, 2001 (2020).